OVER WING PROPELLER AERODYNAMICS

R K Cooper, W J McCann and A Q Chapleo

Department of Aeronautical Engineering,
Queen's University of Belfast.
Belfast. U.K.

Abstract

The over-wing propeller configuration is studied using experimental and theoretical methods. The aim is to gain an understanding of the interaction between the propeller and wing, including the effect of trailing edge flap deflection.

The numerical panel method and wind tunnel experiments showed that both lift increase and drag reduction are produced for a range of propeller positions. The maximum increment in lift coefficient occurred with the propeller at the trailing edge and the tip close to the surface. Maximum reductions in drag coefficient were obtained with the propeller in the range 0.4 to 0.6 chord, depending on wing incidence and flap angle.

Introduction

Flying machines of many designs may be found in the pages of Jane's All the World's Aircraft[1], for example. The problem of where to put the engines has always caused controversy, and some ingenious solutions have been proposed, such as over-wing mounting (figure 1).

The Custer 'Channel wing' CCW-5[2] had semicircular inner wings, with the propellers located at the trailing edge of the channels, so that the propeller inflow created reduced upper surface pressure, and increased lift. A maximum lift coefficient of 5 was claimed for this aircraft.

Various flying boats have had the engines and propellers mounted above the wing, to be well clear of the water, notably the ten engined Dornier Do-X of 1929. Recently Dornier have proposed a 1000 tonne 'flying ship'[3], with a span of 108 m, and ten turbofan engines mounted above the wing. The Beriev A-40 Albatross amphibian[1] has a high, swept wing, with twin turbofans mounted above the trailing edge. The VFW-Fokker VFW 614 has turbofans mounted on pylons above a low wing of moderate sweep.

The Antonov An-72 and An-74[1] (and the Boeing YC-14 experimental STOL transport[4]) have two turbofan engines mounted close to the fuselage and exhausting over the wing, to take advantage of the Coanda effect, in which the jet flow remains attached to the upper wing surface when flaps are extended, thus turning the flow.

The Northrop B-2[1] has four jet engines buried in the wing, with over-wing inlets and exhausts. This design is driven by the need to minimise the radar reflections from the turbo machinery, so any favourable aerodynamic interaction is secondary. It is notable that, with the exception of the Antonov An-72 and An-74, few over-wing engined aircraft have been built.

Over wing propulsion

The aerodynamic effects of over-wing jets were studied by Putnam[5,6], and Sawyer and Metcalfe[7], for example. Putnam[5] showed that a jet above the wing increased the lift and reduced the drag of the wing. The key aerodynamic feature was the turbulent jet mixing which entrained free-stream flow over the upper surface, thus decreasing pressure over the leading edge and upper surface, and increasing circulation. Increased jet blowing resulted in an increased distortion of the span load distribution. Increasing the vertical distance of the jet above the wing reduced the favourable interference effects. For twin jets, the closer the jets were to the centre-line, the more favourable were the effects. Fortunately, this feature would also minimise the engine-out rolling moment, as suggested by Phelps and Smith[8]. An experimental investigation by Putnam[6], for jet locations 0.75 to 1.5 diameters above the wing, confirmed the above predictions. He found that the increase in lift was about one-third of that which would be achieved if the jet turning over the wing due to the Coanda effect had been ideal (i.e., equal to the angle at the trailing edge of the wing).

Szodruch and Kotschote[9] investigated the effect of different engine simulations and stub-wing mountings for an over-wing fan-jet aircraft. Ejector driven nacelles were found to be inadequate, when compared with full-scale tests, but Turbo-powered simulators (TPS) were acceptable. They showed that the effect of inflow to the TPS was significant, and thus simulation using externally blown nacelles was inadequate. Substantial lift increase and drag reduction were found at the higher jet velocities, in spite of non-optimal design of the stub wing mounting.

Johnson and White[10] examined the aerodynamics of an over-the-wing propeller configuration (figure 2) to determine whether the propeller inflow velocity was effective in producing favourable interference effects similar to those noted for over-the-wing jet engine configurations[5-9]. Tests at a climb lift coefficient of 0.7 showed significant performance improvements over designs which had the

propeller mounted in front of the wing. They also found that nacelle/wing interference was reduced by positioning the engines well clear of the wing, and that pylon/wing interference was reduced by mounting the pylons on the aft fuselage. The over wing propeller induced flow over the wing, thus reducing drag and increasing lift. Maximum benefit was obtained with propeller location at 20% chord, which produced 20% increase in lift/drag ratio. Compared with a conventional propeller in front of wing location, the slipstream scrubbing drag and nacelle-wing interference problems are avoided.

It is clear from the above research that significant improvements in aerodynamic efficiency may be achieved with over wing propeller configurations. In this paper we report the results of a theoretical and experimental study of over wing propeller aerodynamics, including the effect of flap deflection. The aims were: (i) to develop a numerical model to determine local wing pressures, forces and moments; (ii) to test an over-wing propeller model with a plain flap in the low speed wind tunnel; (iii) to correlate the results of the above.

Panel Method

The British Aerospace panel program SPARV (Source Panel And Ring Vortex)[11] was used to model a simple over wing propeller configuration. SPARV included lifting wing, non-lifting body and lifting nacelle components. Mass flow through the nacelle was modified by a control face component. Facilities for Prandtl-Glauert Mach number correction, wake relaxation, and attached boundary layer prediction, were not used.

There was no propeller model in SPARV, but a propeller was approximated by a nacelle with control face to determine the mass flow. Thus by shaping the nacelle to simulate the streamtube enclosing the slipstream of the propeller, and setting the appropriate velocity of inflow at the control face, it was possible to simulate the velocity field due to a propeller, in particular the inflow to the propeller disk. The velocity increment at the propeller plane was one half of that at the downstream end of the contracting nacelle, where the control face was located. The pressure difference between the inside and outside of the nacelle should be constant, and this condition was used to determine the nacelle shape.

A rectangular wing of aspect ratio 5, with a NACA0012 section was used for all cases. Due to computer limitations, a relatively coarse panelling was required. The wing had 392 panels, arranged in 14 strips, each with 14 panels chordwise on both upper and lower surfaces. A plain flap hinged at 30% chord was modelled for some cases. The axisymmetric nacelle had 224 panels, 16 circumferential by 7 chordwise on each surface; with another 40 panels on the control face. Thus the over wing nacelle configuration had 656 panels. The wing chord and propeller diameter were equal.

Ideally the nacelle would have zero wall thickness, but this was not possible. After some experimentation, a nacelle wall thickness of 1% propeller diameter was selected, with a flared inlet lip extending 1% of diameter ahead of the propeller plane, figure 3. A nacelle length of 52% diameter was found to be sufficient to represent the streamtube contraction. Nacelle shapes were determined iteratively for three propeller thrust coefficients, to satisfy approximately the boundary conditions of tangential flow, constant pressure difference between the inner and outer surfaces, and the appropriate flow velocities at the propeller plane and control face. The propeller thrust loading was thus carried on the inlet lips, contracting surfaces of the nacelle, and on the control face. It is believed that this model gave a sufficiently accurate representation of the outer flow to estimate the interference effect on the wing surface pressures.

The nacelle/propeller was mounted at mid-span above the wing of aspect ratio 5. The nacelle tip was located a fixed distance of 10% chord above the wing surface, for all cases reported herein, since closer locations gave increased upper surface pressures due to the constrained flow between wing and nacelle. Cases for wing incidences of 0, 6 and 12 degrees, with flap angles of 0, 10 and 20 degrees, and chordwise propeller locations from the leading edge ($xp/c=0$) to the trailing edge ($xp/c=1$), with thrust coefficients (based on propeller disk area) 0.51, 0.89 and 1.59, were computed.

Typical chordwise pressure distributions (figure 4) show the effect of propeller at 20% chord, thrust coefficient of 0.89, at various incidence and flap angles. The upper surface pressure on the forward half of the wing is reduced, and the lower surface pressure slightly increased, thus producing increased lift and negative drag increment, due to the leading edge suction.

Pressure distributions were integrated to give lift and drag coefficients. It was found that increments in wing lift and drag coefficients due to propeller thrust were approximately proportional to thrust coefficient, as shown in figure 5. In all subsequent figures, data for a thrust coefficient of 0.89, are presented.

The spanwise distribution of the increment in section lift coefficient, due to the over-wing propeller is given in figure 6, for zero incidence and flap angles. The lift increment is distributed over the whole wing, reducing to 50% of the maximum value about one propeller diameter away from the centre-line. The spanwise distribution of the increment in section drag coefficient is shown in figure 7. Negative increments are generated for all chordwise positions from 0.2 to 0.8 chord. However the 'dips' in the $-\Delta C_d$ distribution near the propeller, for $xp/c=0$, may be incorrect. This effect may be due to blockage by the nacelle/propeller model. The experimental results of Johnson and White[10], figure 15, showed no such dips. Similar dips appear for the trailing edge location.

The increments in wing lift and drag coefficient are given in figures 8 and 9 respectively, for a thrust coefficient of 0.89, for several incidence and flap angles. The lift increment increases with aft movement of the propeller in all cases, but reduces with increasing flap angle. The negative increment in drag is a maximum for propeller positions in the range 0.4 to 0.6 chord. The location of this maximum moves forward with increasing incidence, but moves aft with increasing flap angle.

Experimental Investigation

A pressure tapped wing with NACA 64418 section, 0.302m chord, with a plain flap hinged at 30% chord, was used for the low speed experimental investigation. The wing spanned the minor distance of the 1.14m by 0.86m working section. The two bladed wooden propeller, diameter 0.302m, was driven by an electric motor via a shaft approximately 1 metre long. The propeller and motor drive were mounted on a mechanical force balance, and faired to reduce both parasitic drag, and interference with the wing surface flow. The propeller plane could be positioned above the wing, normal to the wing chord, at any required position, with an accuracy of 1mm. Two values of thrust coefficient (based on propeller disk area), 0.51 and 0.89, were simulated, by setting the required thrust at a constant wind tunnel dynamic pressure. At a constant power setting, the thrust did not vary significantly over the range of positions and incidence (0 to 12 degrees) tested. The Reynolds number (based on chord) was approximately 0.6 million.

For all results presented herein the propeller was positioned to give a tip clearance of 10% of wing chord above the surface with zero flap angle, measured along a normal to the chord line. This position was maintained for deflected flap cases.

The effect of propeller at 20% chord, on pressure coefficient distributions on the centre line, is shown in figure 10, for a thrust coefficient of 0.89. Due to the propeller inflow, the pressure coefficient is reduced on the forward 30% of the upper surface, but increased on the remainder. There is a small increase in pressure on the lower surface.

The sectional lift coefficient is shown in figure 11, as a function of chordwise propeller position, for several spanwise stations. The increment in lift coefficient increases with xp/c to a maximum with the propeller at the trailing edge. Over the range of y/c from 0 to 0.5 (corresponding to the propeller radius), the drop in lift coefficient is relatively small. The relative change is similar to that predicted by the panel method, figure 6, at the corresponding position $2y/b = 0.2$. The effect of flap angle is shown in figure 12.

The sectional drag coefficient versus propeller chordwise position is shown in figure 13 for several spanwise stations. The negative increment in drag coefficient increases with incidence, and also with flap angle, as shown in figure 14. The value of $-\Delta C_d$ is a maximum with the propeller located in the mid-chord region, and the position of the maximum moves forward with increased incidence. The magnitude of the increment reduces with lateral displacement from the propeller centre line, although it was not possible to obtain the full spanwise extent in these experiments. Comparable data derived from the results of Johnson and White[10], figure 15, shows the increment in drag coefficient, normalised by thrust coefficient, versus spanwise station y/c. Note that the effective spanwise influence is about 3 propeller diameters. An approximate relationship between the increments in wing and section drag coefficients, depending on aspect ratio, is

$$\Delta C_D \quad AR/\Delta C_{d\,\max} \approx 1.5$$

The experimental and panel method predictions for the increments in sectional lift and drag coefficients are compared in figures 16 and 17 respectively. Although the wing sections are different, the sectional lift coefficients on the centre line with power off are approximately 0.5 and 0.6 for numerical and experimental models respectively. The experimental increment in $-\Delta C_d$ is about twice as large as the predicted value, but the variation with propeller position is similar. We conclude that the panel method underestimates the effect of the over wing propeller on lift and drag. This may be due to the neglect of entrainment by the propeller slipstream, or the turning of the slipstream by the wing. However these effects are much smaller for the over wing propeller than the over wing jet engine case.

Model Aircraft Flight Tests

Stability and control effects of over-wing propeller configurations were considered by Johnson and White[10]. Their three surface configuration, figure 2, exhibited an unstable break in the pitching moment at the stall, followed by severe nose-up pitch at higher angle of attack. The application of power produced a stabilising influence on post stall pitch-up, and reduced the tendency to a deep stall. We did not have the facilities for similar research, so a different approach was taken, via a student project[12].

A radio controlled model aircraft with an over wing propeller configuration (figure 18) was built to evaluate stability, control and performance effects. The model was modified from a Precedent Highboy III trainer kit. The engine (OS 35 FP, 6cc), fuel tank and throttle servo were mounted on a light alloy plate, which was attached to the wing by four struts. The pusher propeller, diameter 113% of wing chord, was located at 50% chord, with a tip clearance of about 3% chord. A tractor propeller may have been more efficient, but the centre of mass would then have been too far aft. The wing of span 1.5 m, aspect ratio 6.67, was mounted on top of the fuselage, which was extended to accomodate a nose weight, sufficient to

locate the centre of mass at about 20% chord. Elevator, rudder and throttle were controlled.

The aircraft flew reasonably well, but with one notable defect in stability. With power off, a pronounced dutch roll motion with a frequency of about 1 Hz, made landing hazardous. This was due to the blanking of the fin by the wake from the engine assembly. With level flight power, the propeller slipstream enhanced the fin effectiveness and restored stability. The fin area was increased by 30% (figure 18), and power-off lateral dynamic stability was satisfactory. The longitudinal dynamic stability was excellent, as predicted.

It was expected that change in pitching moment due to power may require a large elevator angle to trim. However, applying power did not cause a significant nose-down pitch, due to the increased downwash over the tailplane. With fixed elevator angle, applying power caused the aircraft to climb, thus full control with rudder and throttle was possible. Manoeuvres such as stall turns, barrel rolls, loops, stalls and spins were performed with ease, and safe recovery. The only detrimental effect on performance was due to the high drag of the over wing engine and fuel tank, and this could be reduced by fairing. Unfortunately it was not possible to obtain a quantitative measure of the performance for the over wing propeller model aircraft.

We conclude that there seem to be no additional stability or control problems for over wing propeller aircraft, when compared with similar conventional configurations.

Conclusions

Over wing propeller configurations were investigated by a panel method and by wind tunnel tests. The panel method model used a thin section nacelle, with an internal sink face, to represent the inflow to, and the contracting slipstream from a propeller. Various chordwise positions of a single over wing propeller and NACA0012 section wing of aspect ratio 5, were computed. Wind tunnel measurements of pressure distributions on a wing of NACA 64418 section, with an over wing propeller, were obtained.

The over wing propeller induced flow over the wing, thus causing increased lift and reduced drag. The increment in section lift coefficient increased as the propeller position was moved aft to the trailing edge. The computational results showed a decreased lift increment with increased flap angle. The limited experimental results showed that an increase in incidence or flap angle reduced the increment in section lift coefficient. The favourable, negative increment in sectional drag coefficient increased with both incidence and flap angle, and was a maximum for propeller position in the range 0.4 to 0.6 chord, taking more foward positions with increased incidence. The efficiency of the propeller was maintained, thus the aerodynamic interaction was favourable.

Flight tests on a radio controlled model with over-wing propeller showed no adverse effect on stability or control.

There are significant aerodynamic benefits due to the over wing propeller configuration, as shown by the experimental design of Johnson and White[10], figure 2, and supported by the present data. The main features of the aerodynamic interaction may be predicted approximately by a panel method[11].

References

1. Jane's All the World's Aircraft 1990-91. Jane's Information Group, Coulsdon, Surrey, U.K.

2. Jane's All the World's Aircraft 1960-61.

3. Aerospace, c.1986.

4. Jane's All the World's Aircraft 1978-79.

5. Putnam, L. Exploratory investigation at Mach numbers from 0.4 to 0.95 of the effect of jets blown above a wing. NASA TN D-7367, 1973.

6. Putnam, L. Jets located more than one jet diameter above a wing at subsonic speeds. NASA TN D-7754, 1973.

7. Sawyer, R.A. and Metcalfe, M.P. Jet/ wing interference for an overwing engine configuration. AGARD CP-285, 1980.

8. Phelps, A.E. and Smith, C.C. Wind tunnel investigation of an upper surface blown jet flap powered lift configuration. NASA TN D-7399, 1973.

9. Szodruch, J. and Kotschote, J. On the aerodynamics of over-the-wing nacelles supported on stub wings. AIAA 21st Aerospace Sciences Meeting. 1983.

10. Johnson, J.L. and White, E.R. Exploratory low speed wind-tunnel investigation of advanced commuter configurations including an over-the-wing propeller design. AIAA-83-2531, 1983.

11. Petrie, J.A.H. Userguide for the SPARV panel program. British Aerospace PLC, 1985.

12. Hempsey, P. and Walker, T. Investigation of an over-wing propeller configuration. Final year project report, Dept. Aero. Eng., Queen's University, Belfast. 1989.

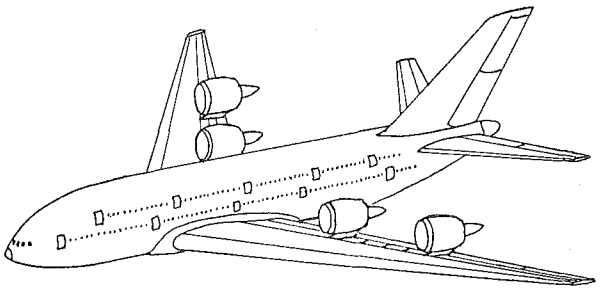

Fig.1. Large transport aircraft concept with over-wing engines.

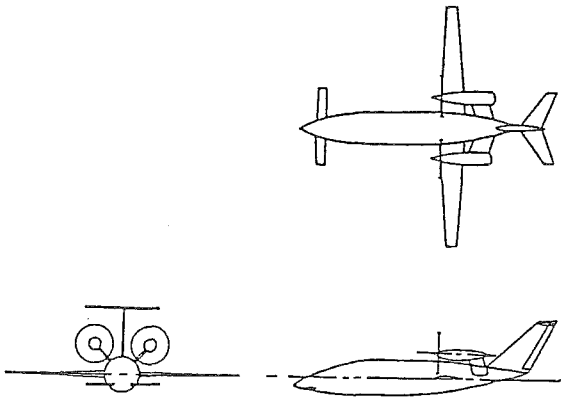

Fig.2. Experimental over-wing propeller design of Johnson and White.

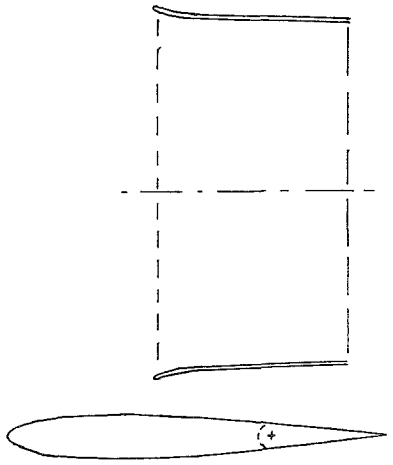

Fig.3. Over-wing nacelle/propeller and NACA0012 wing; panel method model.

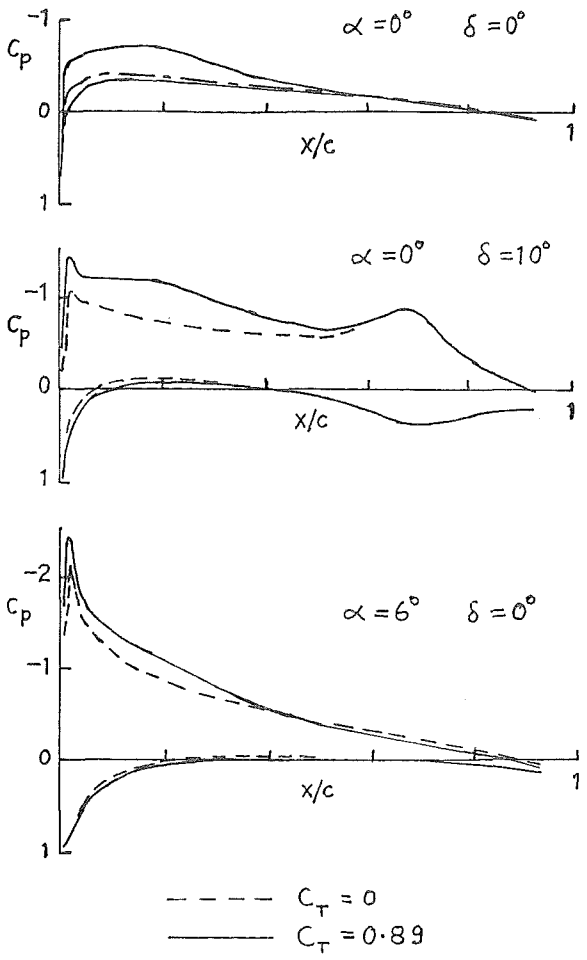

Fig.4. Pressure coefficient distributions on centre line of wing of aspect ratio 5 with over wing propeller: SPARV panel method.

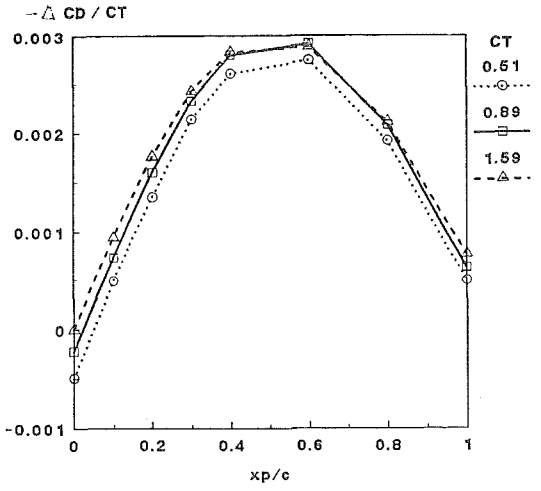

Fig.5. Increment in wing drag coefficient / thrust coefficient vs span station: SPARV panel method. C_T=0.51, 0.89, 1.59 $\alpha = 0°$, $\delta = 0°$

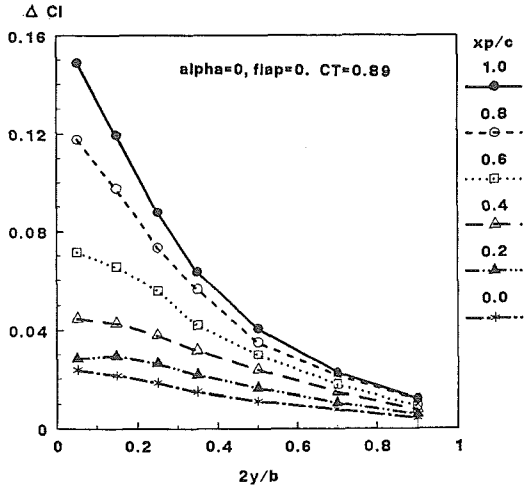

Fig.6. Increment in section lift coefficient vs span station for various propeller chordwise positions.

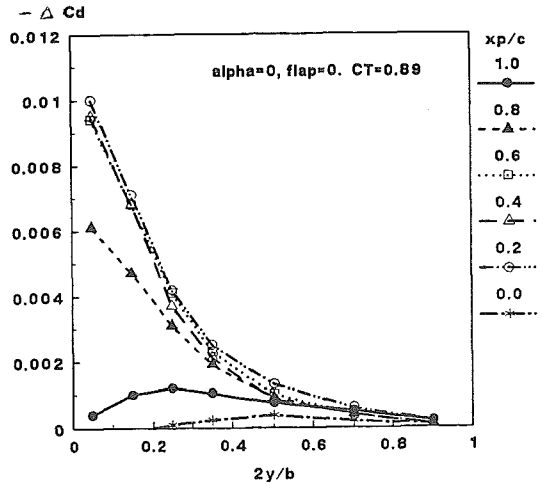

Fig.7. Increment in section drag coefficient vs span station for various propeller chordwise positions.

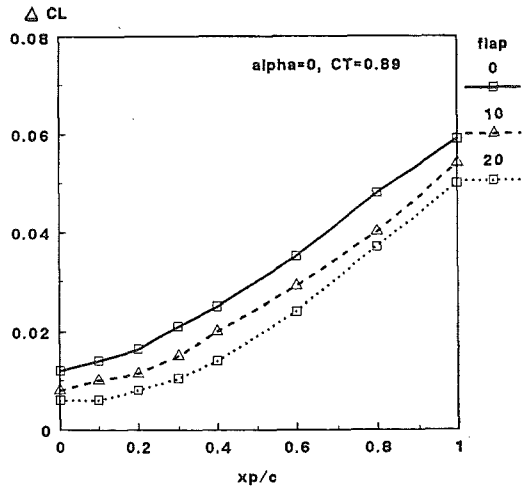

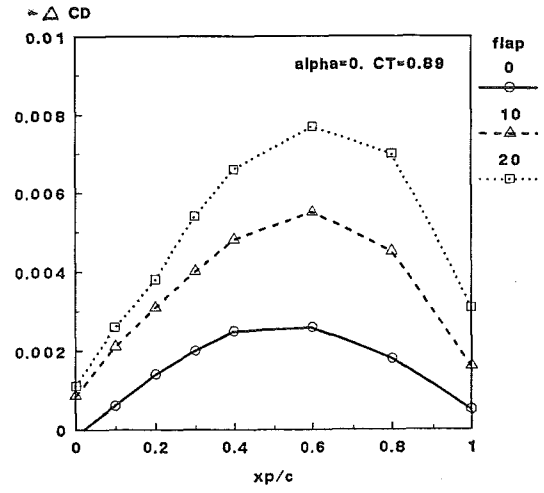

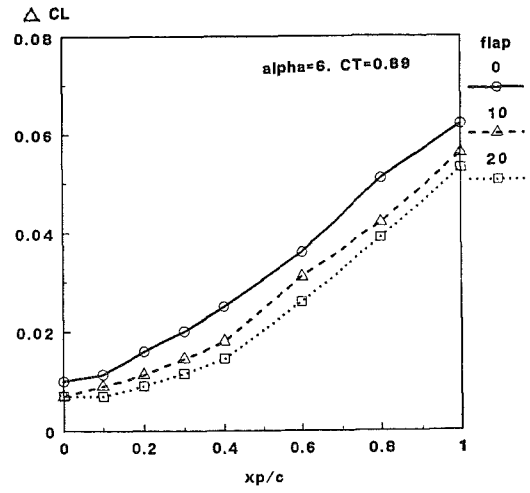

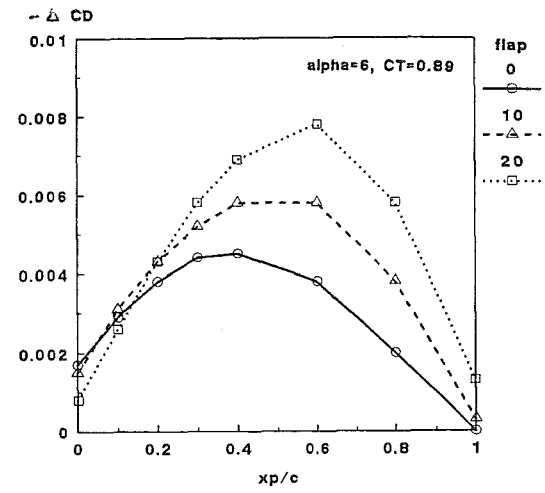

Fig.8. Increment in wing lift coefficient vs propeller chordwise position: SPARV panel method; wing NACA0012, AR=5.
(*a*) $\alpha = 0^\circ$ (*b*) $\alpha = 6^\circ$

Fig.9. Increment in wing drag coefficient vs propeller chordwise position: SPARV panel method; wing NACA0012, AR=5.
(*a*) $\alpha = 0^\circ$ (*b*) $\alpha = 6^\circ$

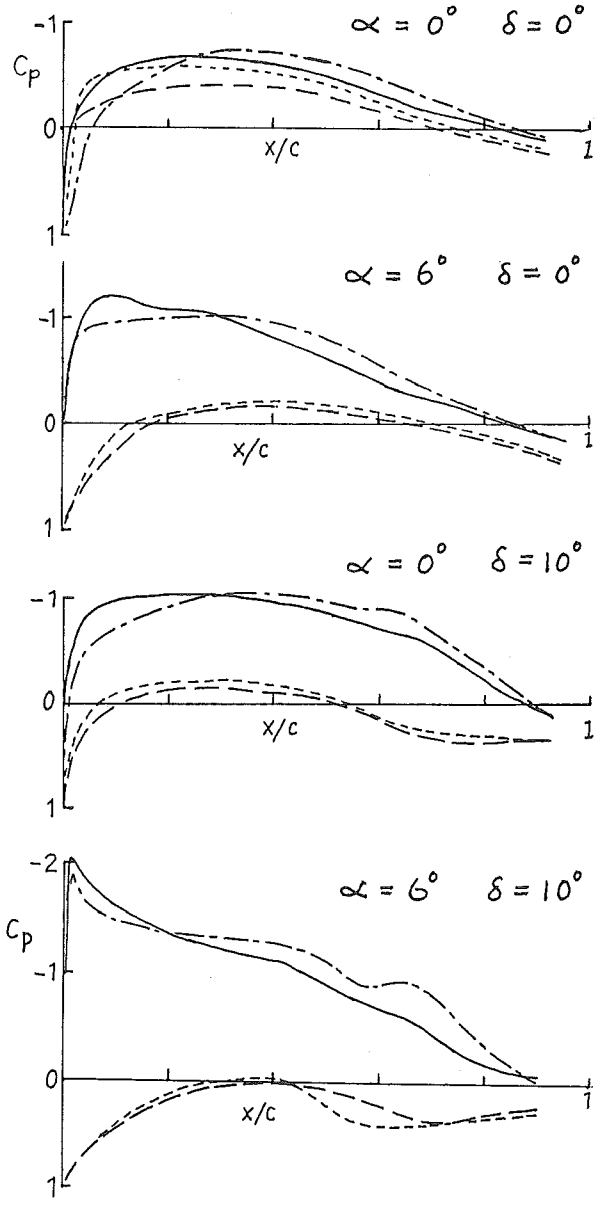

Fig.10 Pressure coefficient distributions on centre line of NACA64418 wing with over wing propeller; wind tunnel data.

C_T=0.0 upper surface – —— –
lower surface – – – –
C_T=0.89 upper surface ———
lower surface —— ——

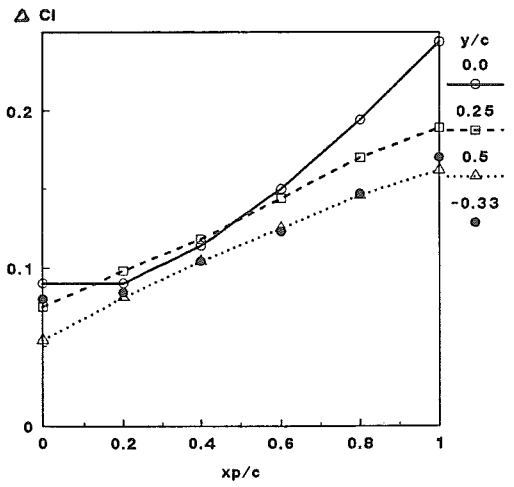

Fig.11 Increment in section lift coefficient vs propeller chordwise position. Wind tunnel data: NACA64418, 2D wing, C_T=0.89
$\alpha = 0°$, $\delta = 0°$

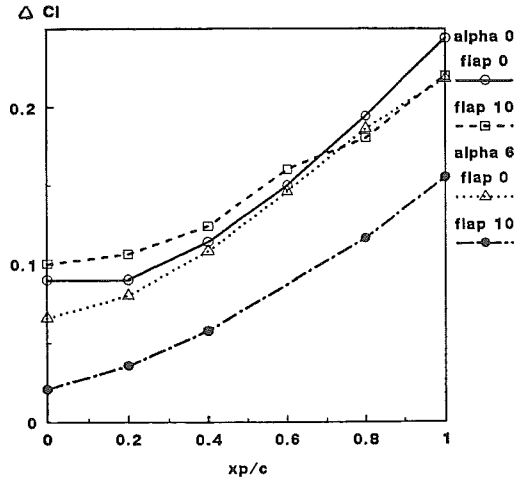

Fig.12 Increment in section lift coefficient vs propeller chordwise position. Wind tunnel data: NACA64418, 2D wing, C_T=0.89, y/c=0.

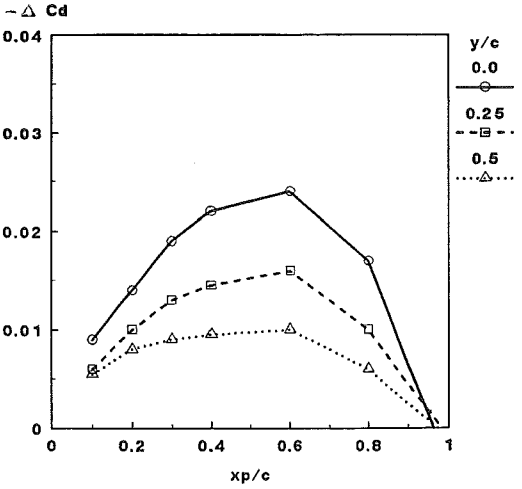

Fig.13(a) Increment in section drag coefficient vs propeller chordwise position. Wind tunnel data: NACA64418, 2D wing, C_T=0.89 .
$\alpha = 0°$, $\delta = 0°$

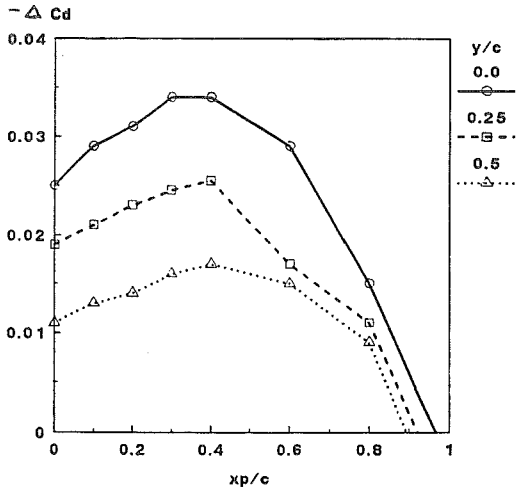

Fig.13(b) Increment in section drag coefficient vs propeller chordwise position. Wind tunnel data: NACA64418, 2D wing, C_T=0.89 . $\alpha = 6°$, $\delta = 0°$

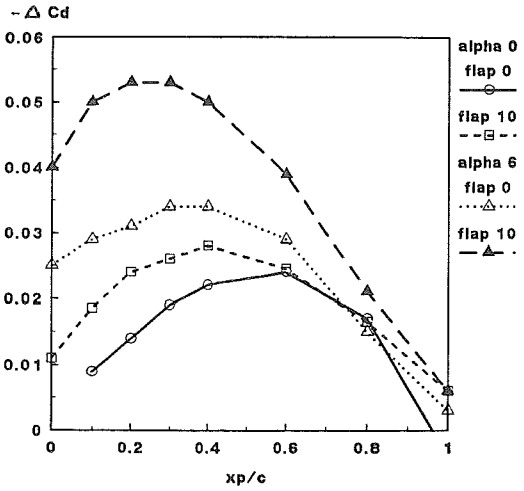

Fig.14 Increment in section drag coefficient vs propeller chordwise position. Wind tunnel data: NACA64418, 2D wing, C_T=0.89, y/c=0.

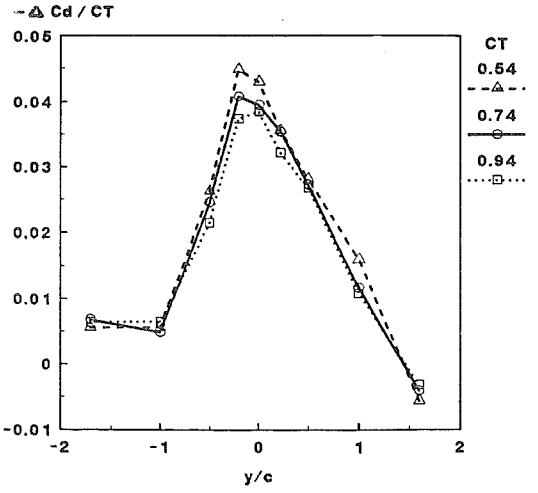

Fig.15 Increment in section drag coefficient/ thrust coefficient vs span station: from wind tunnel data of Johnson and White. Wing: LS(1)0417, AR=5.25, xp/c=0. $\alpha = 6°$

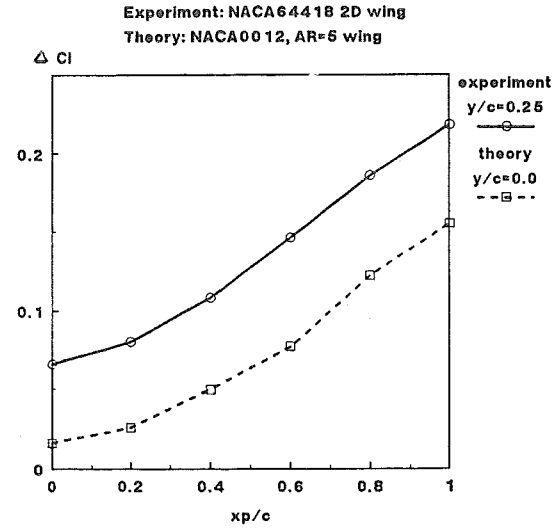

Fig.16 Comparison of theory and experiment for increment in section lift coefficient on the wing centreline vs propeller chordwise position. $\alpha = 6°$, $\delta = 0°$, $C_T = 0.89$.

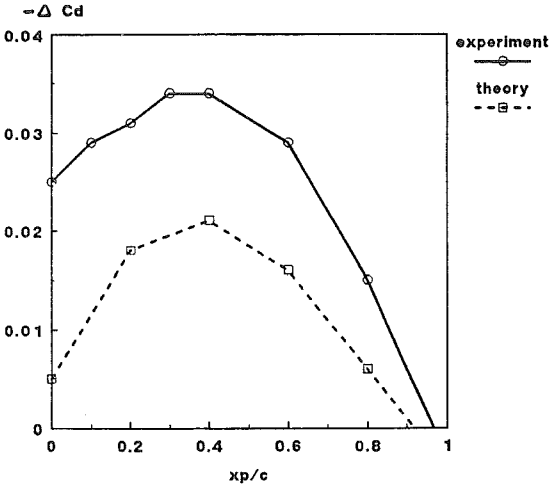

Fig.17 Comparison of theory and experiment for increment in section drag coefficient on the wing centreline vs propeller chordwise position. $\alpha = 6°$, $\delta = 0°$, $C_T = 0.89$

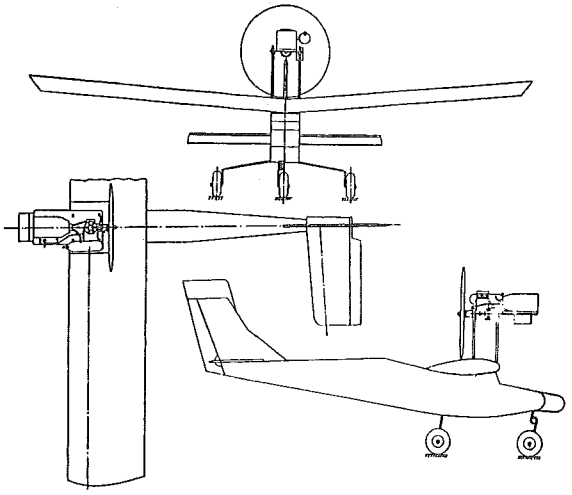

Fig.18 Radio controlled model aircraft with over-wing propeller.